

Citation for published version:

C. Wang, S. Chang, and H. Wu, 'Lagrangian Approach for Simulating Supercooled Large Droplets' Impingement Effect', *Journal of Aircraft*, Vol. 52 (2):524-537, March 2015.

DOI:

<https://doi.org/10.2514/1.C032765>

Document Version:

This is the Accepted Manuscript version.

The version in the University of Hertfordshire Research Archive may differ from the final published version. **Users should always cite the published version.**

Copyright and Reuse:

Copyright © 2014 by the American Institute of Aeronautics and Astronautics, Inc. All rights reserved.

This manuscript version is distributed in accordance with the Creative Commons Attribution Non Commercial (CC BY-NC 4.0) license, which permits others to distribute, remix, adapt, build upon this work non-commercially, and license their derivative works on different terms, provided the original work is properly cited and the use is non-commercial. See:

<http://creativecommons.org/licenses/by-nc/4.0/>

Enquiries

If you believe this document infringes copyright, please contact the Research & Scholarly Communications Team at rsc@herts.ac.uk

A Lagrangian Approach for Simulating Supercooled Large Droplets Impingement Effect

C. Wang¹ and S. Chang²

Beijing University of Aeronautics and Astronautics, Beijing 100191, China

H. Wu³

School of Engineering, University of the West of Scotland, Paisley, PA1 2BE, United Kingdom

In this article, a droplet tracking method (DTM) and a splashing model have been developed to calculate the droplet collection efficiency in super-cooled large droplets (SLD) regime using the Lagrangian computational method. In DTM, the droplet deformation and the droplet-wall effects (e.g. splashing, bouncing and re-impingement) which are the typical cases in SLD regime are incorporated by introducing the mass residual ratio. The effects of the transition from the conventional small droplets (CSD) impingement to SLD impingement as well as the splashed secondary droplets on the droplet collection are considered in the current splashing model. Performance and capacities of the DTM and the SLD splashing model are validated against the alternative experimental reference data. The mass loss ratio and the mass back ratio are introduced in order to explore the distribution and the quantity of the mass loss and mass back caused by droplet splashing and re-impingement. The predicted results show that the quantity and the distribution range of the mass back ratio on airfoil surfaces are relatively lower than that of the mass loss ratio. A significant mass back is observed when the airfoil is contaminated with ice. No mass loss or mass back is observed beyond the impinging region for the given conditions.

¹ PhD Candidate, School of Aeronautic Science and Engineering.

² Prof., School of Aeronautic Science and Engineering.

³ Lecturer, School of Engineering.

Nomenclature

C_d	=	drag coefficient
d	=	current droplet diameter [μm]
d_0	=	initial droplet diameter [μm]
d_{ref}	=	referred droplet diameter [μm]
d_s	=	splashed (secondary) droplet diameter [μm]
d_{in}	=	incident droplet diameter [μm]
ds_i	=	total separation between the trajectories at impact on the surface [m]
dy_i	=	total separation between trajectories in the control volume in the free stream [m]
$f_{H,f}$	=	splashing mass loss fraction
g	=	gravitational acceleration [m/s^2]
H	=	modified Mundo parameter = $\left(Oh Re_{d,n}^{1.25}\right)^{2.0}$
i	=	control volume number, droplet id number
K_f	=	momentum exchange coefficient
LWC	=	liquid water content [g/m^3]
m_f	=	droplet mass filmed on surface after splash [kg]
m_s	=	droplet splashed mass on impact [kg]
m_d	=	initial incident droplet mass [kg]
m_{re}	=	re-impingement droplet mass [kg]
M_s	=	total mass of droplet splashed out of the control volume [kg]
M_0	=	mass collection of the control volume in the case of excluding droplet splashing and re-impinging effects [kg]
M_{re}	=	total mass re-impinges into the micro control volume [kg]
MVD	=	Median Volumetric Diameter [μm]
n	=	number of the collecting droplets of the control volume, impact frequency
N_D	=	Best number = $4\rho_a(\rho_d - \rho_a)gd_0^3/3\mu_a^2$
N	=	number of the splashed droplet
Oh	=	Ohnesorge number = $\mu_d/\sqrt{d_0\sigma\rho_d}$
Re	=	relative Reynolds number = $\rho_a(u_d - u_a)d/\mu_a$
Re_d	=	droplet Reynolds number = $\rho_d u_d d_0/\mu_d$
$Re_{d,n}$	=	droplet Reynolds number characterized by droplet normal velocity = $\rho_d u_{d,n} d_0/\mu_d$

S	=	airfoil curvilinear length [m]
t	=	time [s]
\mathbf{u}_d	=	droplet velocity [m/s]
\mathbf{u}_a	=	air velocity [m/s]
u_t	=	terminal velocity [m/s]
u_s	=	splashed droplet velocity [m/s]
u_{dx}	=	droplet velocity in the x direction
u_{dy}	=	droplet velocity in the y direction
$u_{d,n}$	=	normal component of droplet velocity
We	=	relative Weber number = $\rho_a (u_a - u_d)^2 d / \sigma$
We_d	=	droplet Weber number = $\rho_a u_d^2 d_0 / \sigma$
$We_{d,n}$	=	droplet Weber number characterized by droplet normal velocity = $\rho_a u_{d,n}^2 d / \sigma$
x, y, z	=	coordinators
Δy	=	initial length between neighboring droplets in the free stream [m]

Greek Letters

α	=	angle of attack, AOA [deg]
β_i	=	droplet collection efficiency
ζ	=	eccentricity parameter = $1 - (1 + 0.007\sqrt{We})^{-6}$
η	=	residual ratio = m_f / m_d
θ_0	=	droplet incident angle [deg]
Λ	=	droplet frequency [1/s]
μ_a	=	droplet shear viscosity [Pa·s]
μ_d	=	air shear viscosity [Pa·s]
ρ_a	=	air density [kg/m ³]
ρ_d	=	droplet density [kg/m ³]
σ	=	surface tension coefficient [N/m]
ψ_{ls}	=	mass loss ratio
ψ_{bk}	=	mass back ratio

Abbreviation

CFD	=	Computational Fluid Dynamics
-------	---	------------------------------

<i>CSD</i>	=	Conventional Small Droplet
<i>DPM</i>	=	Discrete Particle Model
<i>DTM</i>	=	Droplet Tracking Method
<i>SLD</i>	=	Super-cooled Large Droplets
<i>SIMPLE</i>	=	Semi-Implicit Method for Pressure Linked Equations
<i>TP</i>	=	terminal point
<i>UDF</i>	=	User-Defined Function
<i>WSU</i>	=	Wichita State University

Subscripts

<i>a</i>	=	air
<i>b</i>	=	bouncing
<i>cr</i>	=	critical
<i>d</i>	=	droplet
<i>i</i>	=	id number, control volume number
<i>n</i>	=	the component in the normal direction
<i>ns</i>	=	no splashing
<i>ns-re</i>	=	re-impingement without splashing
<i>re</i>	=	re-impingement
<i>ref</i>	=	referred
<i>s</i>	=	splash term
<i>s-re</i>	=	re-impingement with splashing
<i>t</i>	=	the component in the tangential direction
<i>0</i>	=	initial

I . Introduction

AIRCRAFT icing due to super-cooled large droplets (SLD), *e.g.* freezing drizzle and freezing rain, with median volumetric diameter (MVD) larger than 50 μ m has taken on more serious potential hazards in airplane flight than the conventional small droplet (CSD, MVD \leq 50 μ m) [1-3]. SLD tend to splash on impact creating a large number of smaller droplets which are also referred to as the secondary droplets

increasing the potential for ice contamination on unprotected surfaces. Therefore, droplet splashing has increased the randomness of the droplet impingement. Prediction of the droplet collection efficiency, which is the essential part of ice accretion simulation, has thus become a challenging issue in SLD regime.

To the best of authors' knowledge, the earliest issues on the SLD dynamics *e.g.* droplet deformation, breakup, splashing and bouncing are reported by Papadakis et al. [4-6]. Their experimental results show that the significant discrepancies of the droplet impingement curves are found between the numerical and the experimental data. And the reason for the higher numerical predictions could be mainly attributed to less consideration of the SLD dynamics, especially the mass loss due to droplet splashing. According to this, experiments on SLD dynamics have been expanded in order to obtain a better understanding of the dynamics of large droplets collisions with aircraft [7-9]. On the numerical side, methods and models developed in Lagrangian [10] or Eulerian [11] frame of reference are always applied to calculate the droplet collection efficiency in CSD regime. However, the Lagrangian approach is more common in SLD regime, as droplet deformation, both the splashing and bouncing effects are basically Lagrangian in nature. Although the mass deposition and loss due to droplet splashing can be modeled in an Eulerian modelization through source or flux terms [12-14], the droplet splashing and the re-impingement of the secondary droplets are rather difficult challenges to be solved with a field approach. Recently, a significantly computational cost has been reported when droplets re-impingement is considered in Eulerian framework [15]. This work describes the methods and the models to perform the droplet collection efficiency calculations in SLD regime for the Lagrangian approach.

In Lagrangian simulation of SLD impingement, the WSU (Wichita State University) splashing

model which is obtained by applying appropriate curve-fit equations to the predicted droplet impingement efficiency [5, 16] is developed [17-18]. However, this model is not widely used since it requires a high level of details of the key parameters in the model correlations. Afterwards, another tentative model which is referred to as the LEWICE splashing/bouncing model is presented [19, 20]. This model is a modified version of Trujillo splashing model [21] and the significant characteristic of the model is that if droplets impinge perpendicularly to the surface, no matter whether splashing occurs or not, the predicted quantity of the mass loss is zero. Details of other splashing models as well as their performance in SLD regime are summarized in [22]. Additionally, it is suggested that the droplet splashing and the bouncing are the first-order effects on SLD impingement curve predictions while the droplet deformation and the breakup are the second-order effects [19, 22].

Based on the above experimental and numerical investigations, it can be concluded that the mechanism of SLD impingement is quite complicated and much efforts are still needed to model SLD phenomenon and it is therefore imperative to develop more practical methods in SLD impingement computation. In the current study, a new approach based on the Lagrangian method as well as a splashing model is developed to calculate the droplet impingement in SLD regime. In the proposed approach, the droplet deformation drag, the splashing/bouncing and the re-impingement effects will be taken into account through semi-empirical correlations. The approach and the splashing model are validated against a set of experimental data reported by Papadakis et al. [6, 23]. Finally, the mass loss and the mass back (re-impingement) on airfoil surfaces will be addressed.

II. Droplet Trajectory Equation

The following major assumptions are employed in the derivation of the governing equations:

(i) The mass transfer and the resulting momentum exchange between the air phase and the liquid phase are assumed to be negligible;

(ii) No heat transfer or evaporation in the process of droplets movement and impingement. Thus, the thermophysical properties of the droplets are assumed to be constant;

(iii) As the ratio between the air density and the droplet density is very small and droplets do not rotate, the added mass force, the Basset history force, and the Magnus and Saffman forces are all negligible in the present study;

(iv) No inter-droplet collision, coalescence or breakup before impacting on surface and the flow field is unaffected by the presence of the droplet. Other simplifications are described in the due course in the rest of the paper.

A. Droplet Motion Equation

When a droplet is subjected to flow with relative velocity, the forces induced by their motion relative to the continuous phase are followed. The force balance equates the droplet inertia with the forces acting on the particle, and can be written

$$\frac{d\mathbf{u}_d}{dt} = K_f (\mathbf{u}_a - \mathbf{u}_d) + \frac{(\rho_d - \rho_a)}{\rho_d} \mathbf{g} \quad (1)$$

where $K_f (\mathbf{u}_a - \mathbf{u}_d)$ is the drag force per unit particle mass and

$$K_f = \frac{18\mu_a C_d Re}{\rho_d d^2} \quad (2)$$

Here, \mathbf{u}_d is the droplet velocity, \mathbf{u}_a is the air velocity, t is the time, \mathbf{g} is the acceleration due to gravity, μ_a is the molecular viscosity of the air, ρ_a is the density of the air, ρ_d and d refer to the droplet density and diameter. C_d is the drag coefficient defined in the drag model, see Section B. Re is the relative Reynolds number defined as:

$$Re = \frac{\rho_a (\mathbf{u}_a - \mathbf{u}_d) d}{\mu_a} \quad (3)$$

B. Drag Model

To account for the contribution of the droplet deformation to the drag coefficient in variable flow Reynolds number and Weber number, the following formulation is used

$$C_d = (1 - \xi)C_{d,sph} + \xi C_{d,disk} \quad (4)$$

$$C_{d,sph} = 0.36 + 5.48 Re^{-0.573} + \frac{24}{Re} \quad (5)$$

$$C_{d,disk} = 1.1 + \frac{64}{\pi Re} \quad (6)$$

where $C_{d,sph}$ and $C_{d,disk}$ denote the drag coefficient of the sphere and the disk, respectively, We is the relative Weber number and ξ is an eccentricity function of We . These parameters are given as follows:

$$Re = \rho_a (u_d - u_a) d / \mu_a, \quad We = \rho_a (u_a - u_d)^2 d / \sigma, \\ \xi = 1 - \left(1 + 0.007 \sqrt{We}\right)^{-6} \quad (7)$$

It should be noted that d denotes the current droplet diameter in Eqs. (2), (3) and (7), that is, in case of the droplet splashing, it denotes the secondary droplet diameter, σ is the droplet surface tension coefficient. More details about the sphere and the oblate disk drag laws can be found in Ref. [24, 25].

C. Terminal Velocity

The assumption that the droplet is initially travelling at the same speed as the local air velocity is no longer valid for SLD movement. In SLD regime, the terminal velocity of the droplet should be considered. The terminal velocity of a fluid particle in creeping flow is obtained by equating the total drag to the net gravity force, $4\pi(d_0/2)^3 (\rho_d - \rho_a) g / 3$, giving

$$u_t = \sqrt{\frac{4d_0 g (\rho_d - \rho_a)}{3\rho_a C_d}} \quad (8)$$

where u_t denotes the droplet terminal velocity, d_0 denotes the initial droplet diameter. However, it is not possible to calculate the terminal velocity directly from this relation since the drag coefficient depends also on Re which depends on u_t . To circumvent this difficulty, the Best number N_D presented by Clift et al. [24] is used and which is only a function of physical properties of the droplet and air.

$$N_D = C_d Re^2 = 4\rho_a (\rho_d - \rho_a) g d_0^3 / 3\mu_a^2 \quad (9)$$

More details about the Best number N_D are given in Appendix.

Once the terminal velocity is obtained by Eq. (8), the initial conditions of the droplet velocity can be expressed as:

$$\left. \begin{aligned} u_{dx} &= u_{ax} + u_T \sin \alpha \\ u_{dy} &= u_{ay} - u_T \cos \alpha \end{aligned} \right\} \quad (10)$$

where u_{ax} (u_{dx}) and u_{ay} (u_{dy}) denote the local air (droplet) velocity component in the x-direction and y-direction, respectively; α denotes the angle of attack (AOA).

III. Droplet Tracking Method (DTM)

When the droplet trajectories calculation is finished, the start and impact positions are available. The local value of the droplet collection efficiency, β_i , of the control volume i on the airfoil solid surface is then obtained using the definition illustrated in Fig. 1

$$\beta_i = \frac{dy_i}{ds_i} \quad (11)$$

where ds_i is the total separation between the trajectories at impact on the surface, dy_i is the total separation between the trajectories in the control volume in the free stream and it can be further expressed as

$$dy_i = (n-1)\Delta y \quad (12)$$

here n is the total number of the droplets collected in the control volume, Δy is the initial length

between neighboring droplets in the free stream. In SLD impingement, droplet splashing and re-impingement may occur at the same time and even at the same position. The total mass collected in one control volume may be composed of the incoming mass from far field and the splashed secondary droplets. At this point, the conventional method described above cannot be used directly to calculate the droplet collection efficiency in SLD regime. For this reason, the residual ratio definition is introduced to solve the problem.

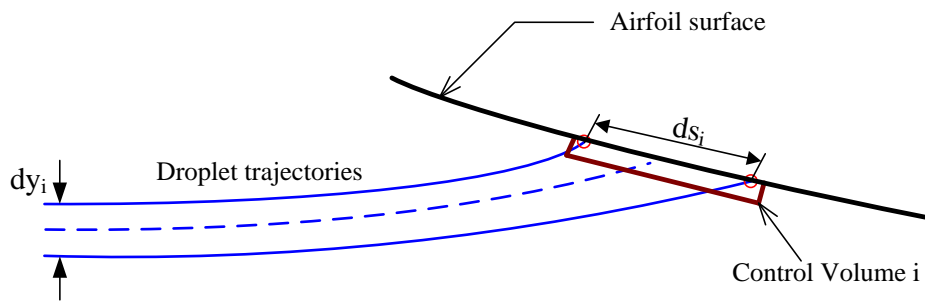


Fig. 1 Droplet trajectories and droplet collection of the control volume i

C. Residual Ratio

For a single droplet impact, the residual ratio η is defined as the ratio of the mass sticks on surface, m_f , to the initial mass of the incident droplet, m_d , after impact.

$$\eta = m_f / m_d \quad (13)$$

The residual ratio on surface can be divided into two categories according to whether splashing/bouncing occurs or not.

(1) No Splashing

Two cases are considered in this impingement type, as shown in Fig. 2. In Fig. 2(a), for the initial impingement, all the incident mass sticks on surface, then the residual ratio is

$$\eta_{ns} = 1 \quad (14)$$

For the re-impingement case, as shown in Fig. 2(b), the residual ratio is given as

$$\eta_{ns-re} = m_{re} / m_d \quad (15)$$

where m_{re} denotes the secondary droplet mass.

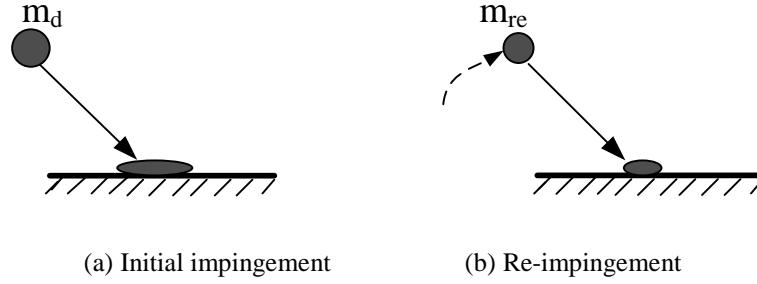


Fig. 2 Droplet-wall interaction without droplet splashing

(2) Splashing

In the case of droplet splashing as shown in Fig. 3, part of the incident mass sticks on surface and part is rejected on impact. Assume the rejected mass is m_s , then the splashing mass loss fraction, f , is given as

$$f = m_s / m_d \quad (16)$$

For the initial splashing case as shown in Fig. 3 (a), the residual ratio is

$$\eta_s = 1 - f \quad (17)$$

The mass loss fraction, f , can be obtained from the splashing model described in Section D. However, if the impact energy is high enough or the solid surface is in a special condition such as covered with a thin film which is always the case for the icing surface, secondary splashing may also occur, as shown in Fig. 3 (b). Then the residual ratio is

$$\eta_{s-re} = \frac{m_{re}}{m_d} - f \quad (18)$$

Droplet bouncing can be deemed as a special case of splashing, all the incident mass is rejected from

surface as shown in Fig. 3(c), thus the residual ratio at the impact point is given as

$$\eta_b = 0 \quad (19)$$

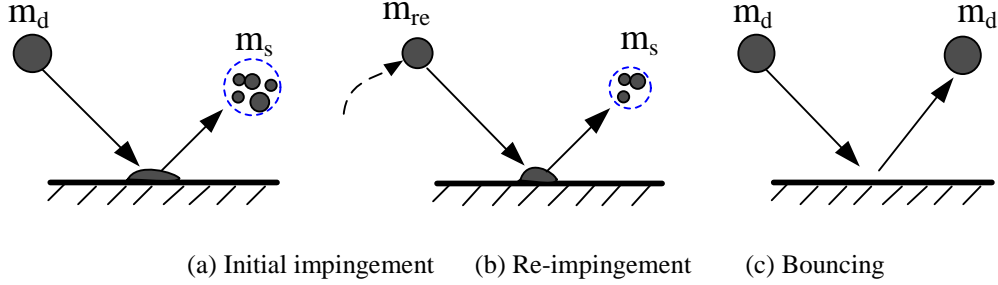


Fig. 3 Droplet-wall interaction with droplet splashing and bouncing

For the micro control volume i laying on the solid surface, it may contain all the impinging types mentioned above. Therefore, the total residual ratio in the control volume i can be expressed as

$$\eta_i = \sum \eta_{ns} + \sum \eta_{ns-re} + \sum \eta_s + \sum \eta_{s-re} + \sum \eta_b \quad (20)$$

where \sum denotes the sum of the residual ratio for the same impinging type within the control volume. Then the droplet collection efficiency of the micro control volume i , incorporated with the effects of droplet splashing/bouncing and re-impingement, can be written as

$$\beta_i = \eta_i \frac{dy_i}{ds_i} \quad (21)$$

D. Splashing Model

Many splashing models exist in spray area (reciprocating engines, gas turbines, spray cooling systems, ink-jet printing, *etc*) [21, 27-29], but if these models are applied to predict the mass loss caused by SLD impingement directly, it will yield a very high mass loss and does not agree well with the experimental results presented by Papadakis et al. [23]. The reports of [12, 17, 19] have shown that the splashing mass loss fraction f must be a decreasing function of the incident angle and the normal component of the incident droplet velocity, in order to be able to account for the experimental results obtained by NASA [4, 23]. After several times of trying to fit the mass loss ratio with the experimental

database [4, 23, 29], a new splashing model which has been modified by Han et al. [29] as well as Trujillo et al. [21] is proposed. In the current splashing model, both the droplets splashing ($0 < f < 1$) and the bouncing ($f = 1$) are coupled and the effects of the transition from the CSD impingement to SLD impingement as well as secondary droplets on the droplet collection are considered. The components of the modified version are described as follows.

(1) Splashing Threshold

$$H = \left(Oh Re_{d,n}^{1.25} \right)^{2.0} > 20 \quad (22)$$

where H is a modified Mundo parameter [28, 29] represented as a function of the droplet Reynolds number $Re_{d,n}$ and Ohnesorge number Oh which are defined as $\rho_d u_{d,n} d_0 / \mu_d$ and $\mu_d / \sqrt{d_0 \sigma \rho_d}$, respectively. Noting that the parameters of $u_{d,n}$ and ρ_d in the droplet Reynolds number denote the normal component of velocity and density of the incident droplet, respectively.

(2) Mass Loss Correlation

The mass loss prediction is modified by Han et al [29], their original correlation is presented in Eq. (23) and the modified version is given as Eq. (24). The effects of the incident droplet diameter, including the secondary droplet, and the velocity on the droplet collection efficiency have been incorporated in the splashing model, see Eqs. (25)-(27).

$$f_H = \frac{m_s}{m_d} = 0.75 \left\{ 1 - \exp \left[-10^{-7} (H - H_{cr})^{1.5} \right] \right\} \quad (23)$$

where H_{cr} denotes the criteria of droplet splashing in Ref. [29]. The modified version of the expression is given as:

$$f = \frac{m_s}{m_d} = 0.75 \varphi_1 \left(d_0 / d_{ref} \right) \varphi_2 \left(\sin \theta_0 \right) \varphi_3 \left(We_{d,n} \right) \cdot \left\{ 1 - \exp \left[- \left[\left(\cos \theta_0 \right)^{0.125} \Lambda \right]^{-0.4} (H - 20)^{-0.22} \right] \right\} \quad (0 \leq f \leq 1) \quad (24)$$

where

$$\varphi_1(d_0/d_{ref}) = 1 - \exp\left[-0.80 \times (d_0/d_{ref})^{4.0}\right] \quad (25)$$

$$\varphi_2(\sin\theta_0) = 1 + (0.90 \times \sin\theta_0)^{4.0} \quad (26)$$

$$\varphi_3(We_{d,n}) = (1 + 0.07\sqrt{We_{d,n}})^{-6.0} \quad (27)$$

where θ_0 denotes the impact angle between the incident droplet velocity and the surface normal vector (see Fig. 4). d_{ref} denotes the referred droplet diameter and 50 μm is selected as the size of the referred diameter which is also the defined boundary between the CSD and SLD. A is the droplet incident frequency and $We_{d,n}$ is the droplet Weber number characterized by the normal component of the droplet velocity, they are given as:

$$A = 1.5 \cdot (\rho_d/LWC)^{-1/3}, \quad We_{d,n} = \rho_d u_{d,n}^2 d / \sigma \quad (28)$$

One significant characteristic of the splashing model is that for the CSD impingement the mass loss fraction f is increasing with the increase of the incident droplet diameter, while for SLD impingement the mass loss fraction performs a decreasing tendency with the increase of the incident droplet diameter. This behavior is inspired by Honsek et al. [12], Wright [19] and Tan et al. [17]. In Honsek's work, an apparent deviation between the predicted droplet collection efficiency and the experimental data is observed at larger MVDs, and DROP3D shows a lower-prediction on droplet collection efficiency at the leading-edge area. In Tan's reports, a decreasing tendency of the mass loss fraction due to droplet splashing is found with the increase of droplet size in SLD regime. The LEWICE splashing model presented by Wright reports zero mass loss if the droplet impact perpendicularly in the leading-edge area, however, their numerical results [13] show that the LEWICE model over-predicts the droplet collection efficiency in the stagnation point area especially for the impact of the smaller size droplets. Therefore, by combination analysis of the SLD splashing models above, the referred diameter 50 μm with the function $\varphi(d_0/d_{ref})$ is introduced into the current model

to modify the effect of the diameter on the droplet collection efficiency. It should be noted that, for the CSD impingement, the predicted mass loss is of the order of 10^{-2} , while for SLD impingement, it is of the order of 10^{-1} . This is reasonable because many experiments [4-6, 23] have served to demonstrate that the mass loss from splashing is very low for the case of CSD impingement but it performs a significant increasing tendency in the transition stage from the CSD impingement to SLD impingement.

(3) Droplet Size and Velocity Profile

The size of the splashed secondary droplet d_s is determined by Eq. (29). Finally, splashed droplet number N may be determined from the total mass and diameters of the secondary droplets combined with the principle of mass conservation, see Eq. (30).

$$\frac{d_s}{d_0} = \frac{3}{We_d^{0.5} Re_d^{0.25}} \sqrt{\frac{\rho_d}{\rho_a}} \quad (29)$$

$$N = 6m_s / \pi d_s^3 \rho_d \quad (30)$$

where the droplet Weber number $We_d = \rho_d u_d^2 d_0 / \sigma$ and the droplet Reynolds number $Re_d = \rho_d u_d d_0 / \mu_d$. However, due to the limitation of the capacity of the current computation and the complexity in tracking large number of the splashed secondary droplets during splashing, the total rejected mass from surface is assumed to be a mass package, as shown in Fig. 4. Therefore, the rejected diameter and the momentum are finally expressed as $\sqrt[3]{6m_s/\pi}$ and $m_s u_s$, respectively.

The velocity profile of the rejected droplet is described as [21]:

$$\left. \begin{aligned} \frac{u_{s,t}}{u_{d,t}} &= 0.85 + 0.0025\theta_0 \\ \frac{u_{s,n}}{u_{d,n}} &= 0.12 + 0.0020\theta_0 \end{aligned} \right\} \quad (31)$$

where the subscript t and n stand for the components of the droplet velocity in the tangential and

normal directions; s and d denote the droplet splash and the original incident items.

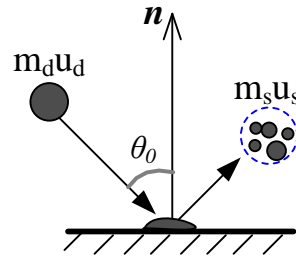


Fig. 4 Mass and momentum change due to droplet splashing.

E. Tracking the Residual Ratio on Solid Surface

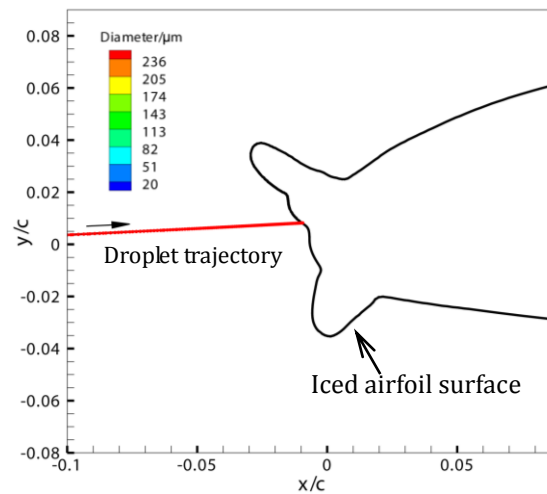
In order to include both the effects of droplet splashing and re-impingement for calculating the droplet collection efficiency, a droplet tracking method has been proposed. Three steps are mainly contained in this method, (1) Classifying According to the Impact Frequency and the Location of the Terminal Point. (2) Calculating the Residual Ratio at the Impact Point. (3) Sum All the Residual Ratio in the Control Volume.

(1) Classifying According to the Impact Frequency and the Location of the Terminal Point

Droplets impinging on the solid surface can be simply subjected to splashing or not. For the case without splashing, the residual ratio is 1, while if splashing occurs, the residual ratio is less than 1 and the induced secondary droplets may partly or totally captured by the solid surface, or totally swept away by the surrounding flow. Therefore, the residual ratio may be varying in different impinging cases. Thus, to identify the impact types has become a necessary step before calculating the SLD collection efficiency. Initially, every droplet is entitled with an id number at the released place and this id number will remain unchanged even in the case of droplet splashing, the id number of the secondary droplet is the same as the parent droplet. When the id number and the coordinates of the impact position (x, y, z) are available, classifying the impact types becomes possible. The location of the terminal point of the

droplet trajectory provides a way to classify the impact types.

According to whether the terminal point (TP) of the single droplet trajectory is located on the solid surface or not, the impact types can be classified into two categories. As shown in Fig. 5, the first is that the TPs are located on the surface. In this case, the total incident droplet, whether droplet splashing or not, is eventually caught by the surface. The solid surface appeared in Fig. 5 is an "iced" airfoil provided by Papadakis et al. [6]. The initial incident droplet diameter is $236\ \mu\text{m}$ and n denotes the impact frequency. Since the rejected mass m_s is varying on splash for different incidents, the splashed diameter ($d_s = \sqrt[3]{6m_s/\pi}$) exhibits different colour as shown in the figures. For the case of $n=1$ as shown in Fig. 5(a), no splashing occurs and this impingement performs the same way with the CSD impingement. For the cases of $n > 1$, as shown in Fig. 5 (b) and (c), re-impingement occurs.



(a) No splashing occurs, $n=1$

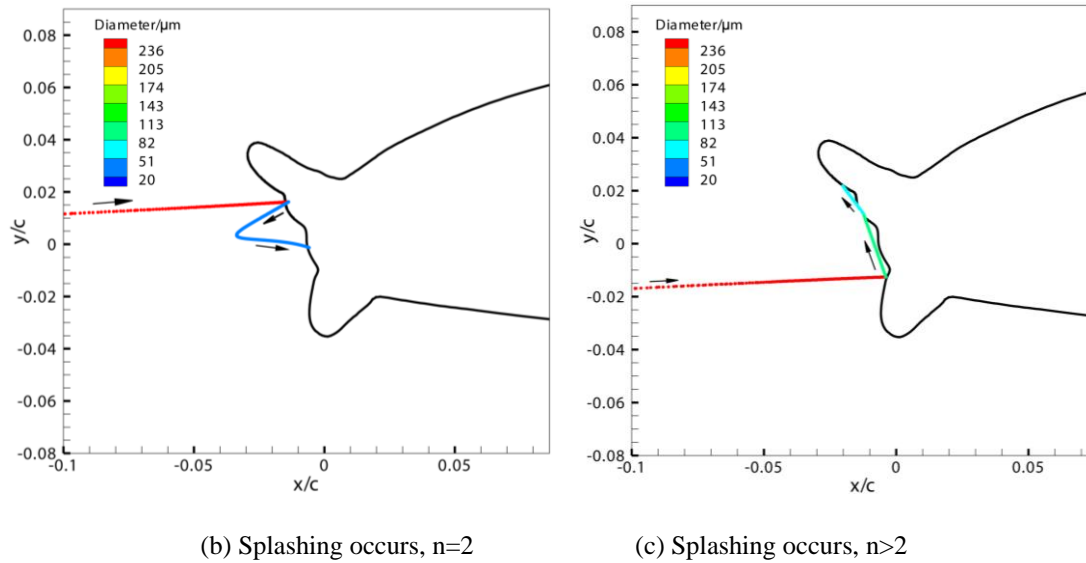
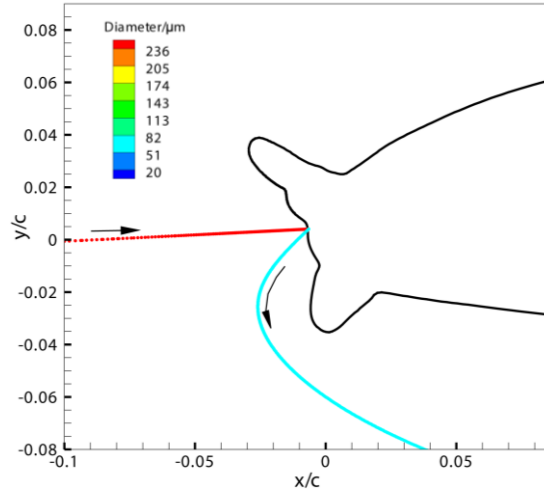
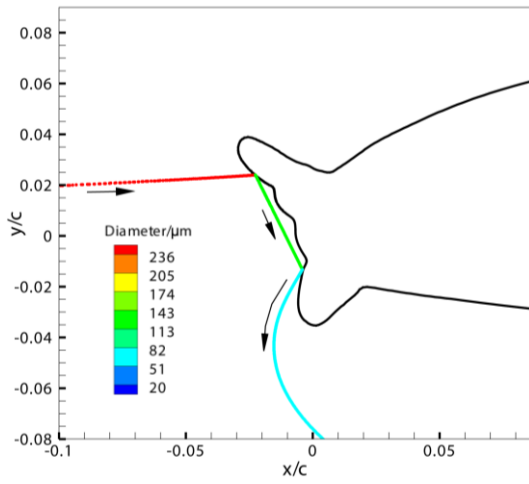


Fig. 5 Droplet trajectory with the TP on the solid surface (MVD=236 μm)

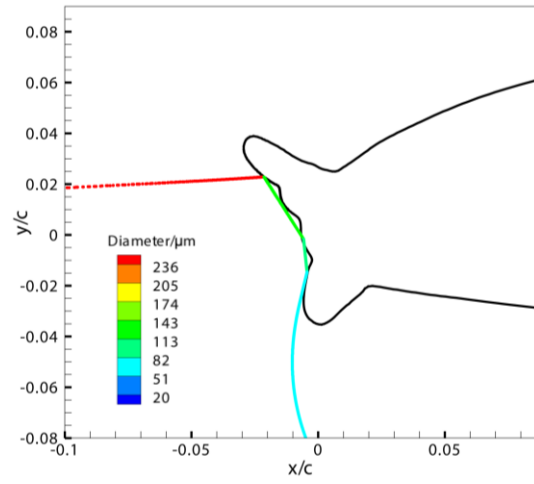
The second category is that after the splashing and re-impingement, part or all the incoming mass, under the influence of the surrounding airflow, finally escapes the solid surface, as shown in Fig. 6. For the first case as shown in Fig. 6 (a), splashing occurs and all the rejected mass flees the solid surface without re-impingement. Droplet bouncing, in which the total incoming mass is rejected from surface, can be classified into this category. For the second and the third cases, as shown in Fig. 6 (b) and (c), droplet splashing and re-impingement occurs at the same time. Finally, part of the secondary incoming mass flees away with the airflow. The quantity of the rejected mass shows a decreasing tendency with the increase of the impact frequency. It should be noted that the impact frequency n is affected by many factors such as velocity, turbulent flow and the bump solid surface. For each impingement, the coordinators of the impact point, the diameters of the parent droplets (d_{in}) and the splashed secondary droplets (d_s) together with the id number $[(x, y, z), id, d_{in}, d_s]$ will be recorded for the following calculation of the residual ratio.



(a) Splashing occurs, $n=1$



(b) splashing occurs, $n=2$



(c) splashing occurs, $n>2$

Fig. 6 Droplet trajectory with the TP out of the solid surface (MVD=236 μ m)

(2) Calculating the Residual Ratio at the Impact Point

Based on the classification and the recorded information $[(x, y, z), id, d_{in}, d_s]$ above, the residual ratio at each impingement can be calculated and located. Fig. 7 shows an incident droplet titled with the id number i impinging on the surface for about three times. At each impingement, it was ticked, *e.g.* 1, 2 and 3, respectively.

At point 1 the residual ratio is given as:

$$\eta_1 = 1 - (d_{i,s1}/d_{i,0})^3 \quad (32)$$

At point 2:

$$\eta_2 = \left(d_{i,s1} / d_{i,0} \right)^3 - \left(d_{i,s2} / d_{i,0} \right)^3 \quad (33)$$

At point 3:

$$\eta_3 = \left(d_{i,s2} / d_{i,0} \right)^3 - \left(d_{i,s3} / d_{i,0} \right)^3 \quad (34)$$

Easy to conclude that if the impingement frequency is more than three times ($n > 3$), the final residual ratio is given as:

$$\eta_n = \left(d_{i,s(n-1)} / d_{i,0} \right)^3 - \left(d_{i,sn} / d_{i,0} \right)^3 \quad (35)$$

Nevertheless, if the TP of the droplet trajectory is located on the surface, the final residual ratio can be expressed as:

$$\eta_n = \left(d_{i,s(n-1)} / d_{i,0} \right)^3 \quad (36)$$

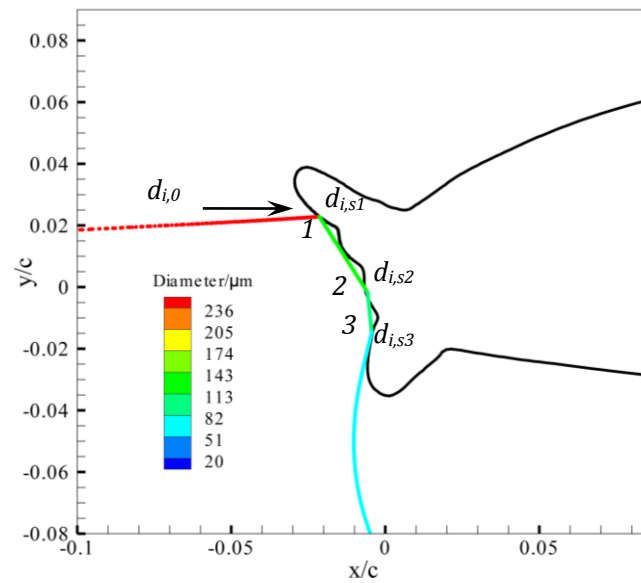


Fig. 7 The splashed droplet trajectory (MVD=236μm)

(3) Sum All the Residual Ratio in the Control Volume

When the first two steps are finished, the information of the mass residual ratio on the solid surface, e.g. $[(x, y, z), id, \eta]$, is available. Based on the coordinators of nodes of the control volumes lay on the solid surface, the residual ratio can thus be “collected” accordingly.

In the current study, we introduce the mass loss ratio ψ_{ls} and the mass back ratio ψ_{bk} in order to better illustrate the mass loss and gain due to the droplet splashing and re-impingement of the control volume, respectively. Both of the two definitions are given as

$$\psi_{ls} = \frac{M_s}{M_0 + M_{re}}, \quad \psi_{bk} = \frac{M_{re}}{M_0 + M_{re}} \quad (37)$$

where

M_s denotes the total mass flows out the micro control volume, *e.g.* splashed mass;

M_{re} denotes the total mass re-impinges into the micro control volume;

M_0 denotes the mass collection of the micro control volume in the case of excluding droplet splashing and re-impinging effects. Thus, $(M_0 + M_{re})$ denotes the total droplet mass that flows into the micro control volume.

F. Numerical Procedure

In the current study, the governing equations of the continuum described by Batchelor [31] are solved with FLUENT (v6.3) general-purpose solver [32]. The analysis employed the SIMPLE algorithm in the software together with the $k-\varepsilon$ RNG turbulence model and near-wall functions. The droplet motion equation described by Eq. (1) is solved with fourth-order Runge-Kutta scheme. The deformation drag model together with the proposed splashing model are incorporated into the governing equations with the help of user-defined function (UDF) and programmed in C code. The macros used are mainly DEFINE_DPM_DRAG and DEFINE_DPM_BC. When the solutions of the droplet trajectories and the droplet-wall interaction are finished, the data of the droplet coordinators, *id* and diameters will become available. In the following step, all the parameters mentioned above will be converted into a data format for application into a DTM code programmed in Visual Basic language. Finally, the droplet collection efficiency is determined according to Eq. (21).

IV. Results and Discussion

In the following sections, the capabilities of the DTM and the splashing model are tested and discussed. The physical models applied in this work are composed of a clean and 22.5-min “iced” Twin Otter airfoils, clean and 22.5-min “iced” NACA23012 airfoils, which are all presented by Papadakis et al. [6, 23]. The range of the droplet diameter varies from 11 μm to 236 μm , that is, the impingement of both the CSD and the SLD impingements are included. Other details of the calculation conditions are given in Table 1.

Table 1 Calculation Parameters

	Twin Otter	“iced” Twin Otter	NACA23012	“iced” NACA23012
Velocity/ $\text{m}\cdot\text{s}^{-1}$	78.25	78.25	78.25	78.25
MVD (d_0)/ μm	11, 21, 79, 168	79, 168	111, 236	111, 236
LWC/ $\text{g}\cdot\text{m}^{-3}$	0.05, 0.19, 0.496, 0.75	0.496, 0.75	0.73, 1.89	0.73, 1.89
AOA/deg	0	0	2.5	2.5
Chord/m	1.448	1.448	0.914	0.914
Pressure/kPa	99.974	99.974	99.974	99.974
Static Tem./K	280.37	280.37	280.37	280.37
References	[17, 23]	[17, 23]	[6, 17]	[6, 17]

G. Droplet Impingement Distribution on the Clean Airfoil Surface

The distribution of the droplet collection efficiency β on the airfoil is calculated using the DTM including or excluding the effects of droplet splashing and re-impingement (namely “Incl. Spl. & Re-imp.” and “Excl. Spl. & Re-imp.” for short). The computed results are validated against a set of data originating from previous studies performed by Papadakis et al. [6, 23] at NASA Glenn’s Icing Research Tunnel. Comparisons of the β plots are also performed with the numerical reference data of LEWICE [6, 23]. The β curves are given as a function of the airfoil curvilinear length “ S ” starting

from the aerodynamic stagnation point of the airfoil ($S = 0$). The negative “ $-S$ ” denotes the lower surface distance from the stagnation point of the airfoil, while the positive “ $+S$ ” denotes the upper surface distance.

(1) Clean Twin Otter Airfoil

Fig. 8 reports the impingement distributions for the four MVDs on the clean Twin-Otter airfoil surface. As the focus of the present paper is put on SLD impingement, therefore, only two size droplets, $MVD=11\mu\text{m}$ and $MVD=21\mu\text{m}$, are applied to test the capability and accuracy of the DTM method in CSD impingement predictions. It can be seen from Fig. 8(a) and (b) that the β curves obtained with DTM performed better agreement with the experimental data throughout the whole impingement region than LEWICE’s results. Both the calculated results and the experimental data are performed a higher collection efficiency at the stagnation point and a gradually decreasing tendency along the chord-wise direction. The predicted maximum droplet collection efficiencies are given as 0.32 ($MVD=11\mu\text{m}$) and 0.52 ($MVD=21\mu\text{m}$), while the corresponding experimental results are 0.33 ($MVD=11\mu\text{m}$) and 0.52 ($MVD=21\mu\text{m}$). Since the mass loss due to the droplet splashing is very low as previously mentioned in Section D(2), both the two β curves, “Incl. Spl. & Re-imp.” and “Excl. Spl. & Re-imp.”, are almost totally coincided throughout the whole impinging region.

For SLD impingements as shown in Fig. 8(c) and (d), however, deviations between the β curves obtained with and without Spl. & Re-imp. are observed. Both LEWICE and the curves excluding splashing & re-impingement effects perform a significant higher prediction over the experimental curves at the stagnation point and in the region where the impinging limits are approached. At MVD of $79\mu\text{m}$, see Fig. 8(c), the β curve obtained with splashing & re-impingement effects shows a perfect agreement with the experimental results throughout the whole impinging region. The maximums of the

predicted and the experimental droplet collection efficiencies are given as 0.74 and 0.73, respectively.

At MVD of 168 μm , see Fig. 8 (d), good agreement is also observed between the Spl. & Re-imp. curve and the experimental curve except for a little deviation in a relatively small region ($S = 0.08$ and $S = 0.2$) on the upper surface. The maximums of the predicted and the experimental droplet collection efficiencies are given as 0.85 and 0.82, respectively. One potential reason for the mismatch could be due to the use of the droplet median volumetric diameter in the computation. Considering the fluctuations in the experiments as reported in [6, 23], therefore, this deviation could not be only attributable to the deficiency of the method or the splashing model.

(2) Clean NACA23012 Airfoil

Another test is performed on the clean NACA23012 airfoil, the numerical results and the experimental reference data are plotted in Fig. 9. Perfect matches between the β curves obtained including splashing & re-impingement effects and the experimental reference data as shown in Fig. 9(a) and (b) have again demonstrated the significant contribution of the proposed splashing model to the improvement of the droplet collection efficiency prediction. In splashing cases, the predicted maximum droplet collection efficiencies are given as 0.87 (MVD=111 μm), 0.96 (MVD=236 μm), and the corresponding experimental results are 0.85 (MVD=111 μm) and 0.95 (MVD=236 μm), respectively. It should be noted that, at MVD=236 μm as shown in Fig. 9(b), the predicted droplet collection efficiencies obtained by including and excluding splashing & re-impingement effects are almost coincident in the vicinity area around the stagnation point, when comparing with the predicted β curves, as shown in Fig. 8(c), (d) and Fig. 9(a). This is because the splashing model gives a lower evaluation of the splashing mass loss with the increase of the droplet size, as previously illustrated in Section D (2). It should be noted that the LEWICE's results are obtained excluding the SLD dynamics

either [6, 23], that's why good matches are also observed between the Excl. Spl. & Re-imp. curves and LEWICE's predictions, as shown in Fig. 8(c), (d), and Fig. 9(a), (b).

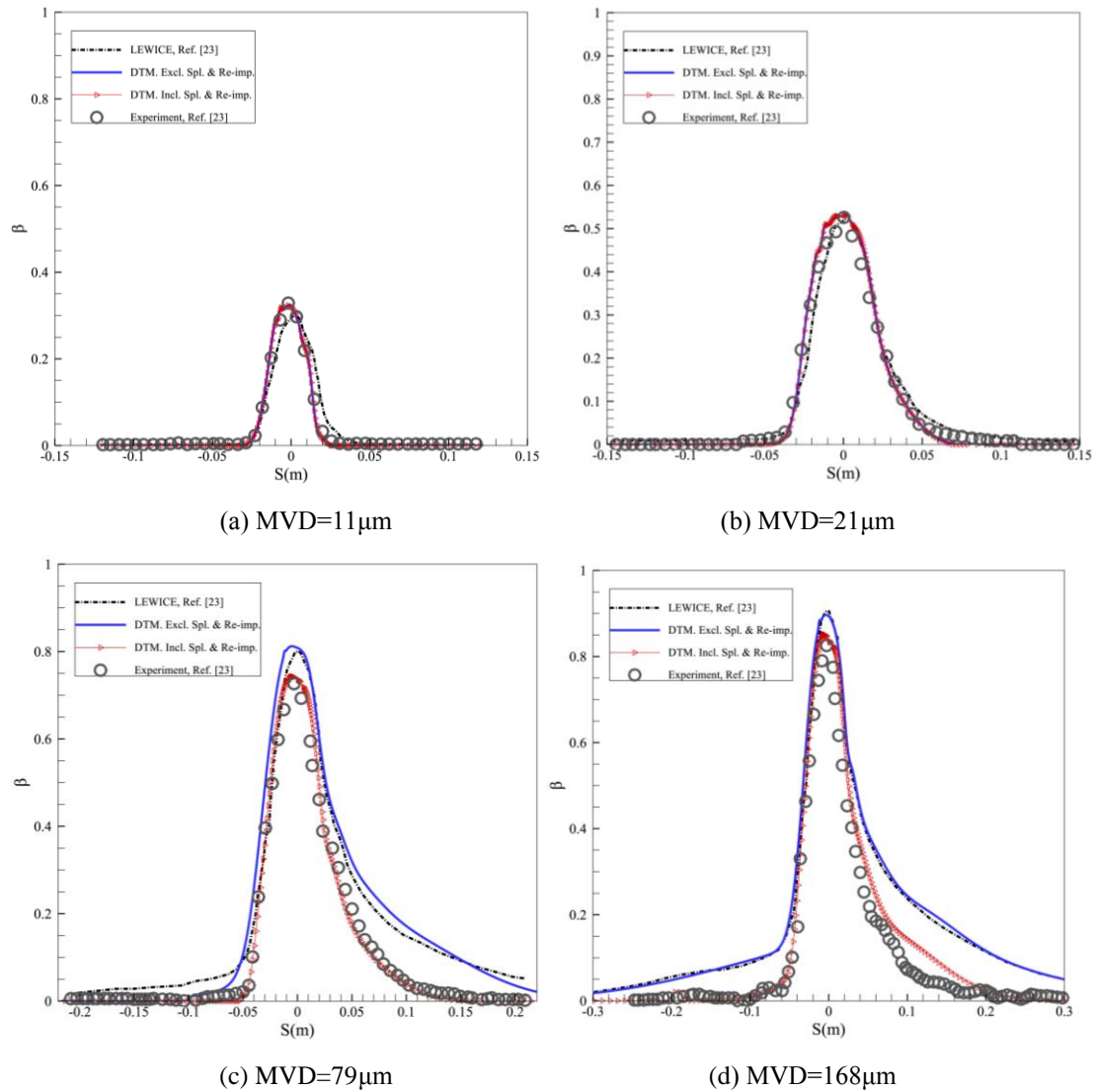


Fig. 8 Comparison of β distribution between computational and experimental results on the clean Twin-Otter airfoil surface

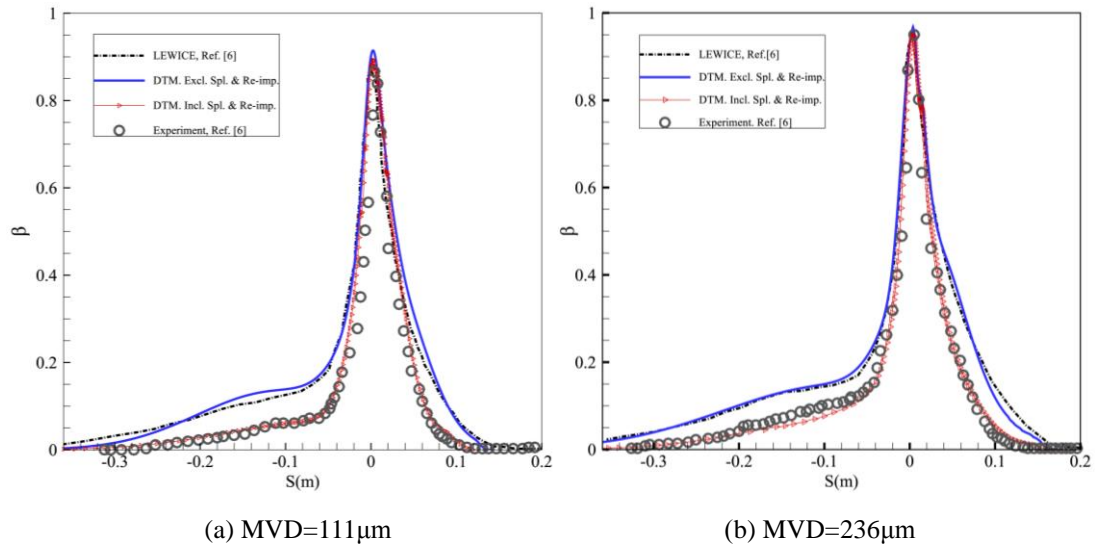


Fig. 9 Comparison of β distribution between the numerical and experimental results on the clean NACA23012 airfoil surface

H. Droplet Impingement Distribution on the Iced Airfoil Surface

In this section, the capacities of the DTM together with the splashing model in predicting the droplet collection efficiency of more complicated surface are examined. The rugged surfaces applied are the Twin Otter airfoil and the NACA23012 airfoil, both with leading-edge double-horn glaze ice contamination after 22.5 minutes [6, 23]. The rugged surface increases the complexity of splashing, bouncing and re-impinging effects which is a more challenging test than the clean ones. The general shapes of the iced airfoils are shown in Fig. 13. The droplet impinging area is divided into two regions, region A and region B, by the ice horns, as shown in Fig. 10. It can be seen that the curves of the droplet collection efficiency have changed greatly when comparing the “iced” β curves with the clean β curves as shown in Fig. 8 and Fig. 9. As expected, both the Excl. Spl. & Re-imp. curves and LEWICE curves give a higher prediction over the experimental reference data in the impinging region especially in region A. However, when the droplet splashing and re-impingement effects are included, the predicted β curves exhibit a significant improvement on the agreement with the experimental

reference data particularly in region A. Nevertheless, in the horn region (region B), a more challenging match between the numerical and the experimental reference data is observed. Although the splashing model is activated, the predicted droplet collection efficiency is still higher than the experimental data for the case of MVD=79 μm impingement as shown in Fig. 10(a). At MVD=79 μm , the predicted maximum droplet collection efficiency in splashing case is given as 0.73 and the experimental result is 0.62. The reason for this mismatch may be attributable to the simple assumption that the rejected secondary mass from surface is taken as a mass parcel, as shown in Fig. 4. Other potential reasons could be attributed to median volumetric diameter in the computation and the fluctuations in the experiments. For the larger size droplet impingements involving 168 μm , 111 μm , 236 μm as shown in Fig. 10(b), (c), and (d), it can be seen clearly that good agreement between the numerical and the experimental reference data are observed when the droplet splashing and re-impingement effects are included. In case of droplet splashing, the predicted maximum droplet collection efficiencies are 0.91 (MVD=168 μm), 0.78 (MVD=111 μm), 0.92 (MVD=236 μm), and the corresponding experimental results are 0.95 (MVD=168 μm), 0.71 (MVD=111 μm), 0.88 (MVD=236 μm), respectively. Close agreements between the numerical and the experimental reference data above allow to be concluded that the DTM incorporated with the splashing model is able to predict the droplet collection more accurately in SLD regime. Droplet splashing and re-impingement effects are relatively strong in the horn regions. Calculation and analysis on the droplet splashing mass loss and the mass back (droplet re-impingement) are expanded in the following sections.

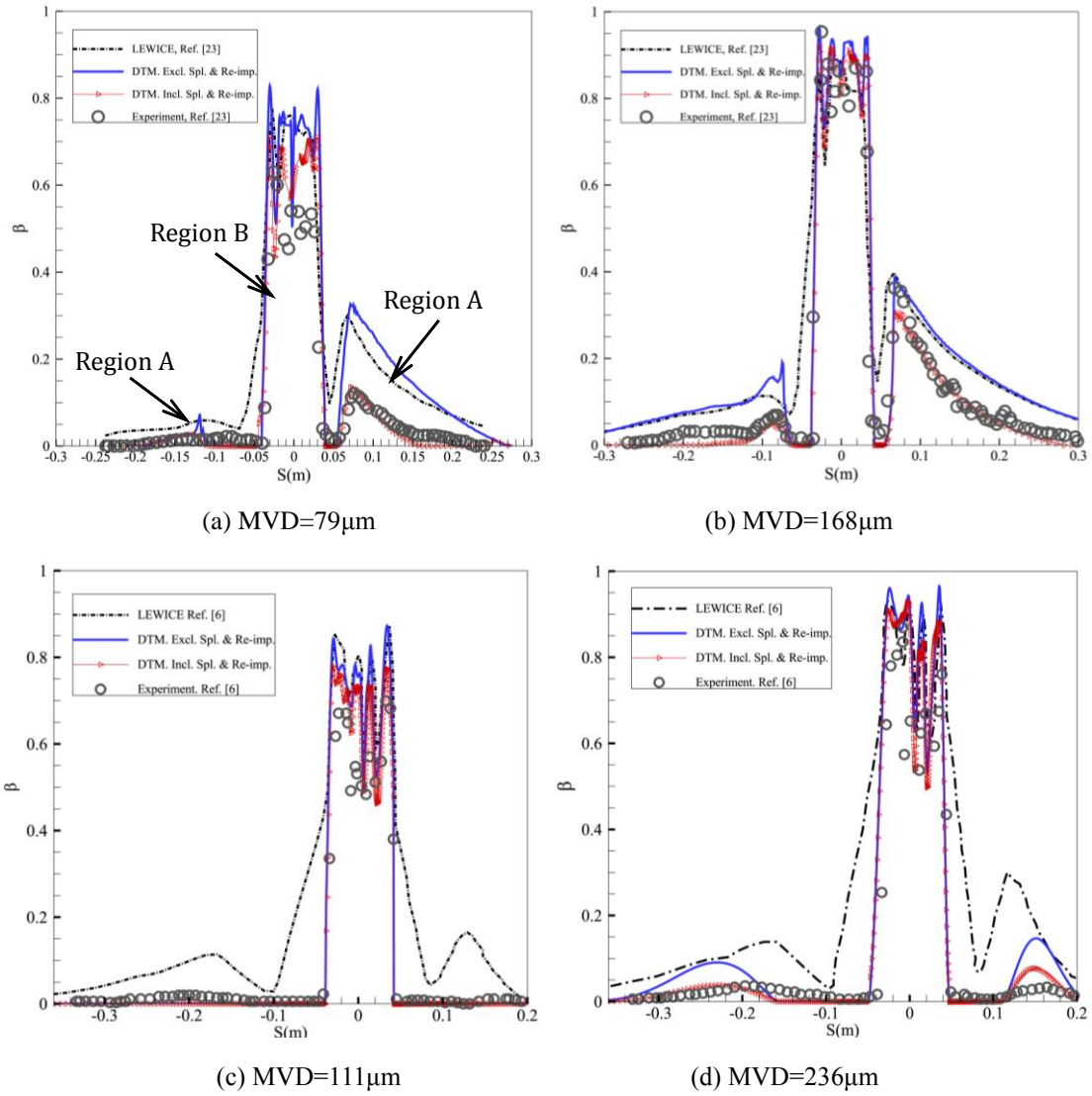


Fig. 10 SLD impingement distributions on the iced airfoil surfaces of the Twin Otter [(a) and (b)] and the NACA23012 [(c) and (d)]

I. Effects of Droplet Splashing and Re-impingement

In this section, the trajectories of the splashed secondary droplets are presented. The distributions of the mass loss ratio and the mass back ratio on the clean and iced airfoil surfaces are calculated and exhibited. The aim is to explore the characteristics of SLD impingement on the airfoil surfaces, which is expected to provide a support for the experimental and numerical simulation of ice accretion in SLD regime.

(1) Trajectory

The effects of surface characteristics on droplets splashing trajectories are presented in Fig. 11. It can be seen that the droplet splashing is occurring almost in the whole impinging region. For the impingement on the clean airfoil, as shown in Fig. 11(a), most of the ejected mass is escaping from the surface when splashing occurs, no significant phenomenon of droplet re-impingement is observed in the vicinity area of the leading edge. However, as shown in Fig. 11(b), for the impingement of droplet on the more complex iced airfoil surface, the re-impingement of the ejected mass on the surface is relatively more significant, especially in the area between the horns. Since the parameters of the incident droplets, *e.g.* the incident angles, velocities and the existing surface curvature, are varying on the solid surface, which make the secondary droplet diameters ejected from the surface is different either, and the figures of droplet splashing are much like a kaleidoscope. It can be seen that the sizes of the secondary droplets are gradually increasing along the chord-wise direction. As the shape of the solid surface is changing with the increase of ice accretion, droplet splashing and re-impingement may play an increasing important role in determining the droplet collection efficiency during the icing process.

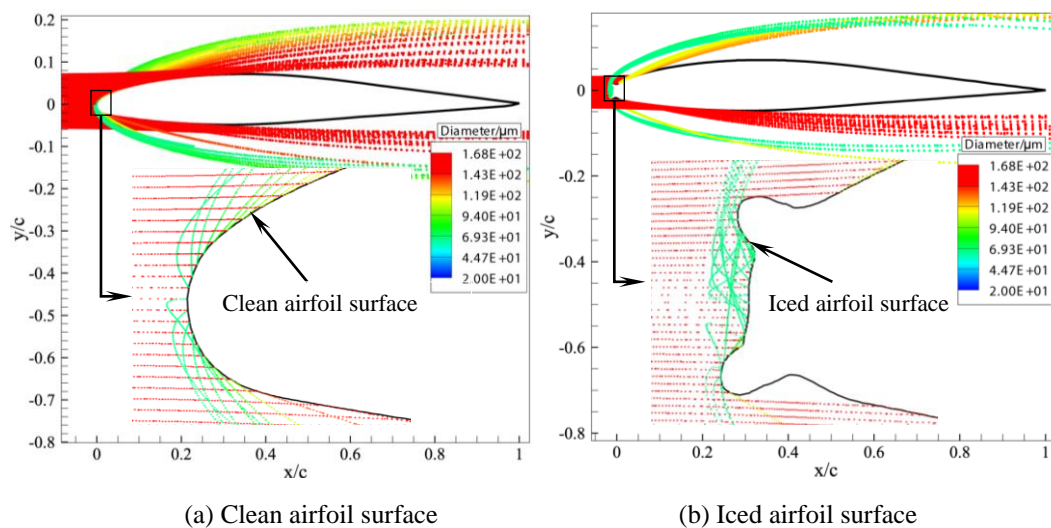


Fig. 11 Droplet splashing and re-impingement on the clean (left) and iced (right) Twin Otter airfoil surface at MVD=168 μ m

(2) Mass Loss Ratio

The mass loss ratio ψ_{ls} denotes the ratio of the quantity of the splashed mass to the total liquid mass collected by the control volume. Fig. 12 demonstrates the distributions of the mass loss ratio on the clean airfoil surfaces. The impingement limits obtained in the condition of excluding droplet splashing and the re-impinging effects are also presented on the airfoil surface. It can be seen clearly that the droplet impinging range is enlarged with the increase of the incident droplet size. The mass loss ratio is relatively lower at the leading edge of the airfoil and performs a general increasing tendency when the impingement limits are approached. At the stagnation point, the mass loss ratio is 0.11 (MVD=79 μm), 0.08 (MVD=168 μm), 0.10 (MVD=111 μm), 0.05 (MVD=236 μm), respectively. A gradually decreasing tendency is observed when the incident droplet diameter is increased for the given conditions. However, the mass loss ratio performs a vibration distribution in the vicinity area near the impingement limits, as shown in Fig. 12(a) and (b). It could be that the droplet splashing and re-impingement occur at the same time in this area. For the impingements of 111 μm , 236 μm as shown in Fig. 12(c) and (d), the mass loss ratio is sharply reduced to zero at the impingement limit points on the upper and lower surfaces.

The distributions of the mass loss ratio on the iced airfoil surfaces are presented in Fig. 13. It can be seen that the distribution of ψ_{ls} in the horn region (region B) is much irregular. It could be the reason that the droplet incident angle has been changed greatly due to the accidented iced surface and thus the mass loss caused by the droplet splashing is influenced accordingly. The level of ψ_{ls} is in the range of 0.05~0.22 in the horn region (region B). At the leeward side of the horns, as no droplet impingement, the mass loss is zero. However, the mass loss ratio performs a similar distribution with the clean surface in the region outside the horns (region A).

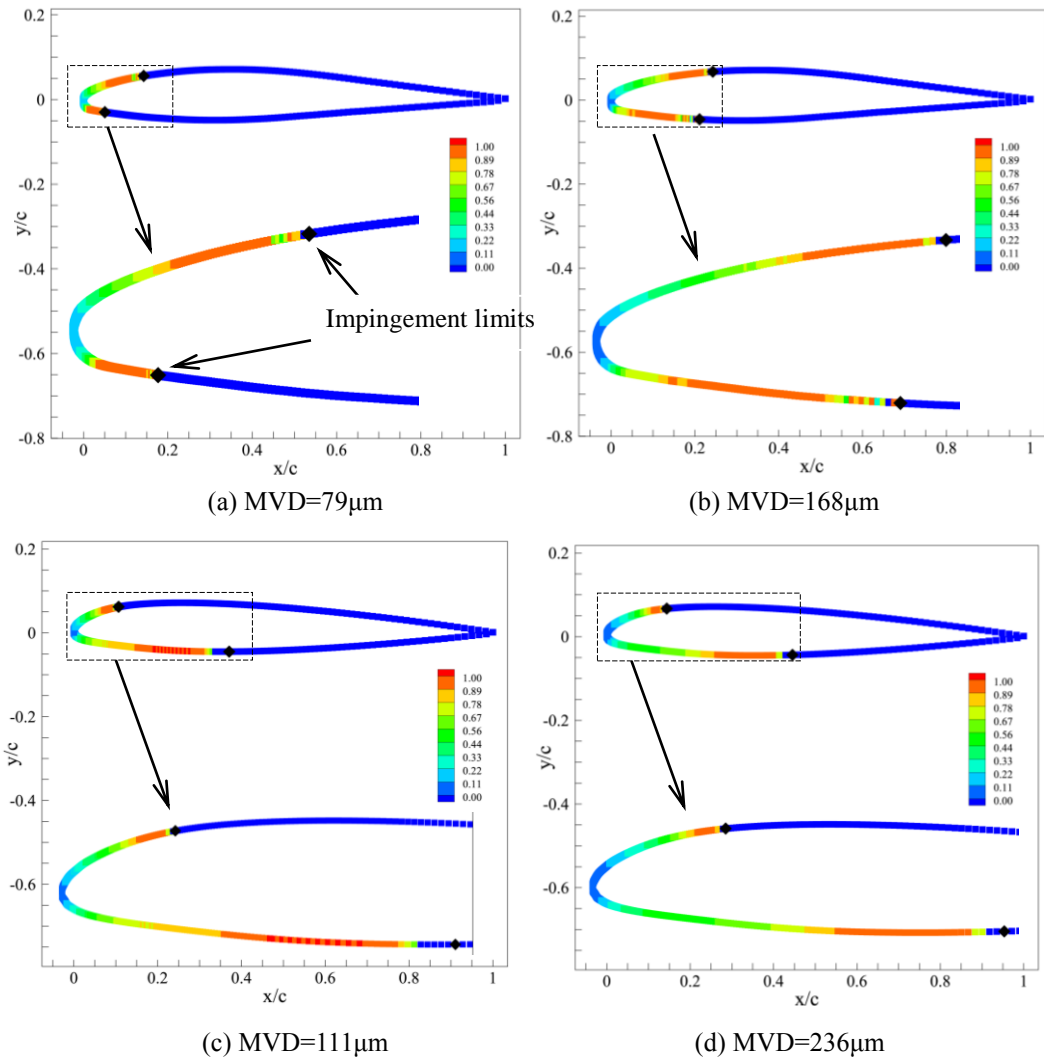
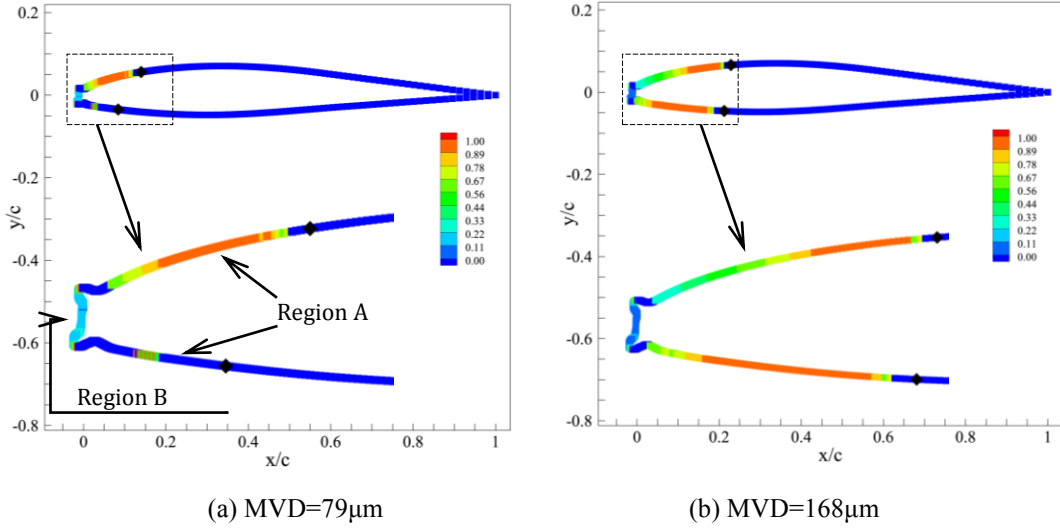


Fig. 12 Mass loss ratio distributions on the clean airfoil surfaces of the twin-otter [(a) and (b)] and the NACA23012 [(c) and (d)]



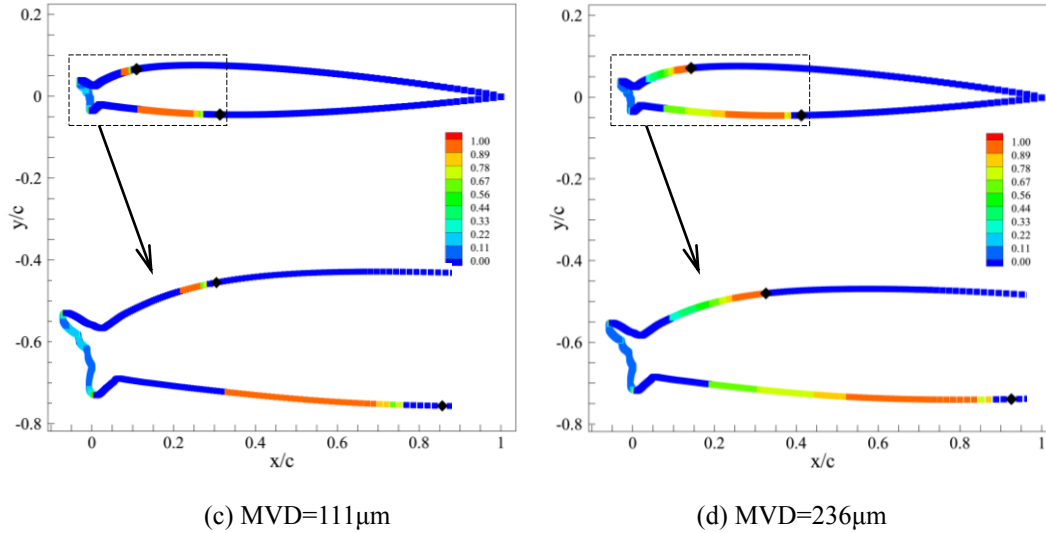


Fig. 13 Mass loss ratio distributions on the iced surfaces of the Twin-Otter [(a) and (b)] and the NACA23012 [(c) and (d)] airfoils

(3) Mass Back Ratio

The mass back ratio ψ_{bk} denotes the ratio of the quantity of the re-impingement mass to the total liquid mass collected by the control volume. The distributions of ψ_{bk} on the clean airfoil surface are presented in Fig. 14. It shows that the range of the ψ_{bk} distribution on the clean surface is relatively narrowed comparing with ψ_{is} , particularly on the NACA23012 airfoil surface, as shown in Fig. 14(c) and (d), no significant mass back is observed. In Fig. 14(a), for the impingement of MVD=79 μ m, a slight mass back on the upper surface is noticed, while for the impingement of MVD=168 μ m in Fig. 14(b), the phenomenon of droplet re-impingement (mass back) is more significant. The results may allow to be concluded that the droplets re-impingement is not only related to environmental conditions but also the shape of the airfoil (length, depth, etc) is playing a key factor. However, when the airfoil is covered with ice horns as shown in Fig. 15, the droplets re-impingement is observed in all the cases and it mainly occurs in the horn region. The distribution level of the mass back ratio ψ_{bk} in the horn region falls in the range of 0~0.22. In all cases, no mass back is observed out of the impinging region. Through the analysis of the distributions of the mass loss ratio and the mass back ratio on the clean and

iced surfaces above, we can see that the effects of SLD dynamics, *e.g.* splashing and re-impingement, on the droplet collection efficiency may be changed greatly due to ice accretion. At this point, it is reasonable to conclude that the multi-step icing simulation is required especially in SLD icing numerical simulation area in order to obtain accurate ice shapes.

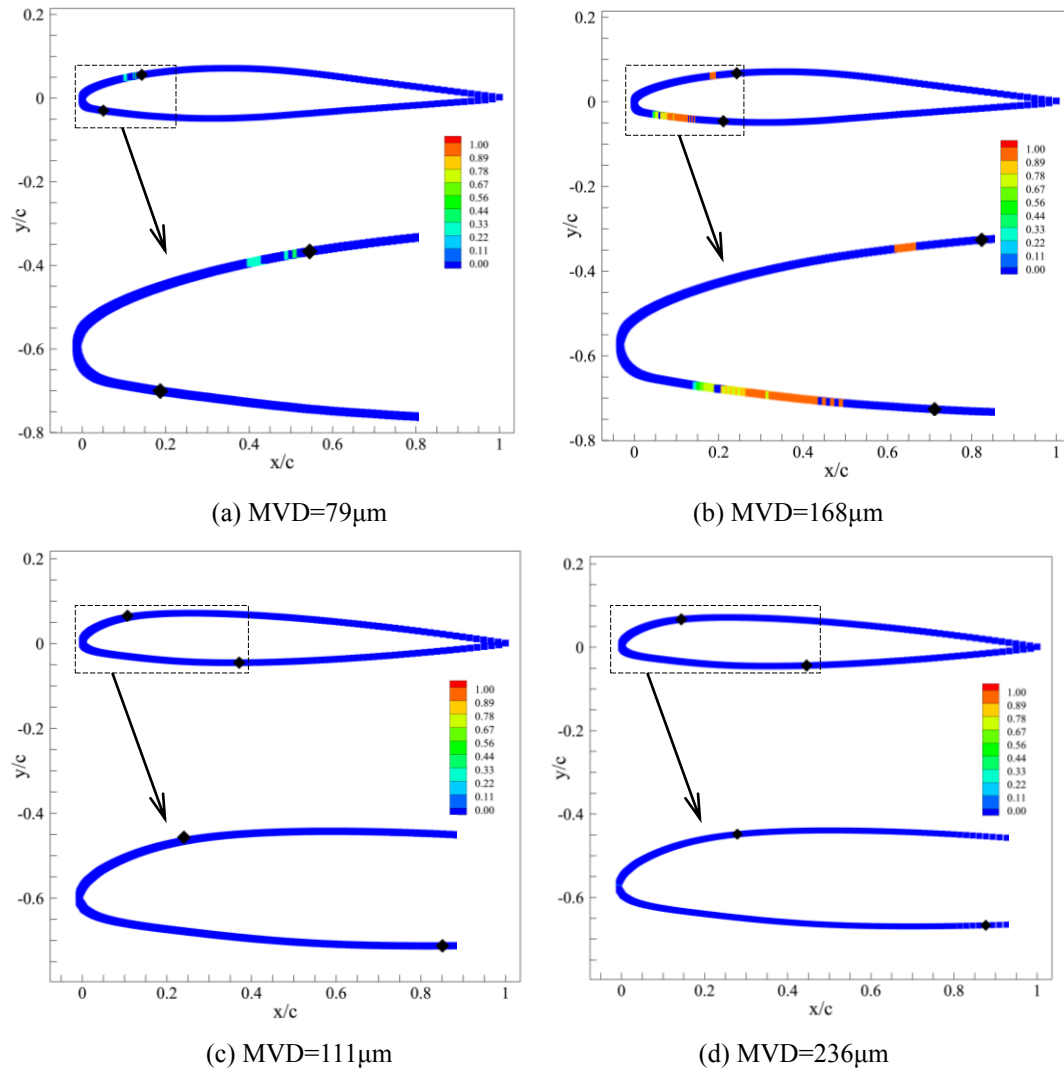


Fig. 14 Mass back ratio distributions on the clean surfaces of the twin-otter [(a) and (b)] and the NACA23012 [(c) and (d)] airfoils

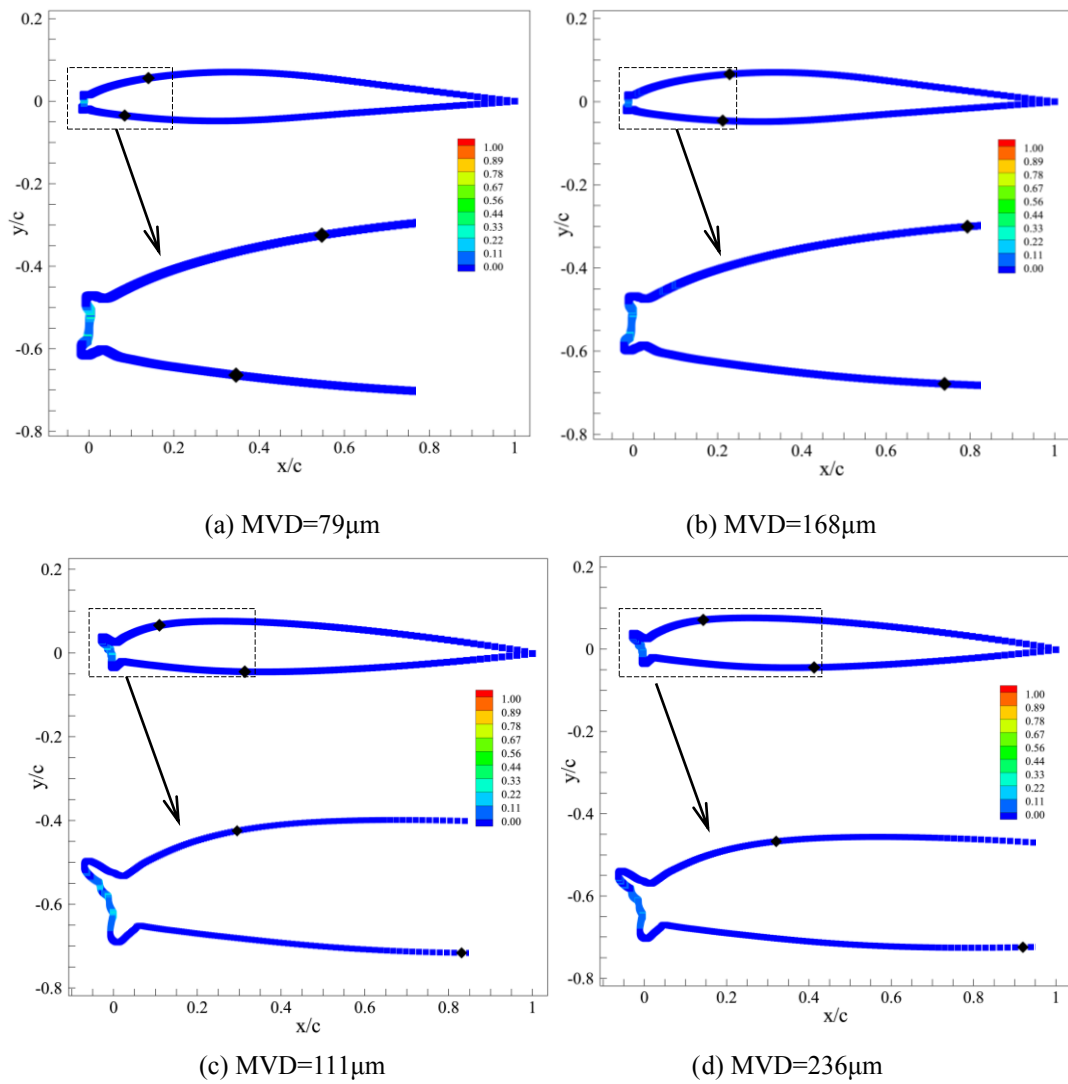


Fig. 15 Mass back ratio distributions on the “iced” surfaces of the twin-otter [(a) and (b)] and the NACA23012 [(c) and (d)] airfoils

V. Conclusions

This article presented an overview of the physical phenomena associated with ice accretion on super-cooled large droplets (SLD), as well as developing a new Lagrangian droplet tracking method (DTM) for the calculation of a two-dimensional droplet impingement, which is applicable in the CSD and SLD regimes. The method has incorporated the effects of the droplet splashing/bouncing and re-impingement by introducing the definition of the residual ratio. A SLD splashing model was

proposed to assess the mass loss during droplet-wall interactions. Capacities and performance of the DTM and the splashing model were validated against a set of experimental reference data available for different airfoils and SLD conditions. The results show that the DTM can predict droplet collection efficiency accurately in SLD regime as well as the CSD impingement. The mass loss predicted by the splashing model has contributed a great deal to the agreement between the numerical and the experimental data. The slight deviations from experimental data observed in the simulation of the validation test cases especially in the iced airfoil conditions maybe attributable either to the use of the droplet median volumetric diameter in the computation or the simple assumption that the rejected secondary mass from surface is taken as a mass parcel or to a deficiency in experimental measurement methods.

The mass loss ratio and the mass back ratio caused by droplet splashing and re-impingement in different SLD impinging conditions were addressed. The mass loss ratio generally performs an increasing tendency from the stagnation point at the leading edge to the area where the impingement limits are approached, but sharp to zero at the impinging limits on the clean airfoil surfaces. At the stagnation point, a generally decreasing tendency of the mass loss ratio with the increase of droplet size is observed at the given conditions. Distributions of the mass loss ratio on the iced airfoil surface are more irregular and it could be attributable to the changes of the droplet incident angle caused by the accidented iced surface and thus the quantity of the mass loss due to splashing is finally changed.

The range and level of the distributions of the mass back ratio on airfoil surfaces are relatively narrowed and lower than that of mass loss ratio and no significant mass back is observed on the clean NACA23012 airfoil at the given conditions. However, when the clean airfoil surfaces are contaminated with horn ice shapes, a significant droplet re-impingement event is observed in the horn region. No

mass loss or mass back is observed beyond the impinging limits at the given conditions. Comparisons of the droplet impingements, the mass loss ratio and the mass back ratio between the clean and iced airfoils serve to conclude that SLD dynamics are affected greatly by surface shapes. Therefore, multi-step icing simulation is thus becoming a strong requirement especially in SLD ice accretion prediction.

Appendix

When more accurate predictions are required C_d vs. Re relationships are inconvenient for determining terminal velocities since both groups involve u_t . Hence an iterative procedure is needed. It is more convenient to express Re as a function of N_D , the latter being independent of u_t . Empirical correlations of this are presented in Table 2 [24].

Table 2 Correlations for Re as a Function of N_D , $W=\log_{10}N_D$

Range	Correlation
(A) $N_D \leq 73; Re \leq 2.37$	$Re = N_D/24 - 1.7569 \times 10^{-4} N_D^2 + 6.9252 \times 10^{-7} N_D^3 - 2.3027 \times 10^{-10} N_D^4$
(B) $73 < N_D \leq 580; 2.37 < Re \leq 12.2$	$\log_{10} Re = -1.7095 + 1.33438W - 0.11591W^2$
(C) $580 < N_D \leq 1.55 \times 10^7$ $12.2 < Re \leq 6.35 \times 10^3$	$\log_{10} Re = -1.81391 + 1.34671W - 0.124271W^2 + 0.006344W^3$
(D) $1.55 \times 10^7 < N_D \leq 5 \times 10^{10}$ $6.35 \times 10^3 < Re \leq 3 \times 10^5$	$\log_{10} Re = 5.33283 - 1.21728W + 0.19007W^2 - 0.007005W^3$

Acknowledgement

This work was financially supported by National Natural Science Foundation of China under Grant No. 11072019. The authors would like to thank Mr. Z. Wenyong and J. Jun for their many contributions to this research.

Reference

- [1] Hansman, R. J., "Droplet Size Distribution Effects on Aircraft Ice Accretion," *Journal of Aircraft* 22, 1985.
doi: 10.2514/3.45156
- [2] Russell Ashenden, William Lindberg, John D. Marwitz, and Benjamin Hoxie., "Airfoil performance degradation by supercooled cloud, drizzle, and rain drop icing", *Journal of Aircraft* 33, 1996.
doi: 10.2514/3.47055
- [3] Charles, M P., "Status of NTSB Aircraft Icing Certification-Related Safety Recommendations Issued As A Result of the 1994 ATR-72 Accident at Roselawn," IN. AIAA, Aerospace Sciences Meeting & Exhibit, 35th, Reno, NV, Jan. 6-9, 1997.
- [4] Papadakis, M, Hung, K. E., Yeong H. W., "Experimental Investigation of Water Impingement on Single and Multi-Element Airfoils," AIAA Paper 2000-0100, 2000.
- [5] Papadakis, M., Hung, K. E., Vu, G. T., Yeong, H. W., Bidwell, C. S., Breer, M. D., and Bencic, T. J., "Experimental Investigation of Water Droplet Impingement on Airfoils, FiniteWings, and an S-Duct Engine Inlet," NASATM2002-211700, Oct. 2002.
- [6] Papadakis, M., Rachman, A., Wong, S. C., Yeong, H.W., Hung, K. E., and Bidwell, C. S., "Water Impingement Experiments on a NACA23012 Airfoil with Simulated Glaze Ice Shapes," AIAA Paper 2004-0565, 2004.
- [7] Tan, S.C., Papadakis, M., Miller, D. Bencic, T., Tate, P., Laun, M.C., "Experimental Study of Large Droplet Splashing and Breakup," AIAA Paper AIAA- 2007-904, 2007.
- [8] Vargas, M., Feo, A., "Deformation and Breakup of Water Droplets near an Airfoil Leading Edge," *Journal of Aircraft* 48, 2011.
doi: 10.2514/1.C031363
- [9] Pierre Berthoumieu. "Experimental Study of Super-cooled Large Droplets Impact in an Icing Wind Tunnel," AIAA Paper, AIAA 2012-3130, 2012.
- [10] Ruff, G. A., Berkowitz, B. M., "Prediction Code (LEWICE). Tech. Rep. CR-185129, NASA," Users Manual for the NASA Lewis Ice Accretion, 1990.
- [11] Beaugendre, H., Morency, F., Habashi, W., "FENSAP-ICE's Three Dimensional In-Flight Ice Accretion Module: ICE3D," *Journal of Aircraft* 40, 2003.
doi: 10.2514/2.3113

- [12] Honsek, R., and Habashi, W. G., "FENSAP-ICE: Eulerian Modeling of Droplet Impingement in the SLD Regime of Aircraft Icing," AIAA Paper 2006-465, 2006.
- [13] Iuliano, E., Mingione, G., Petrosino, F., Hervy, F., "Eulerian Modeling of Large Droplet Physics Toward Realistic Aircraft Icing Simulation," Journal of Aircraft 48, 2011.
doi: 10.2514/1.C031326
- [14] Fossati, M., Habashi, W. G., Baruzzi, G. S., "Simulation of Supercooled Large Droplet Impingement via Reduced Order Technology," Journal of Aircraft 49, 2012.
doi: 10.2514/1.C031326
- [15] Bilodeau, D. R., Habashi, W. G., Fossati, M., Baruzzi, G. S., "An Eulerian Re-impingement Model of Splashing and Bouncing Supercooled Large Droplets," AIAA 2013-3058, 2013.
- [16] Papadakis, M., Rachman A. and Wong, S. C., Bidwell, C. and Bencic T., "An Experimental Investigation of SLD Impingement on Airfoils and Simulated Ice Shapes". AIAA 2003-01-2129, 2003.
- [17] Tan, S.C., "A Tentative Mass Loss Model For Simulating Water Droplet," AIAA Paper AIAA-2004-410, 2004.
- [18] Tan, S. C., and Papadakis, M., "Droplet Breakup, Splashing and Re-Impingement on an Iced Airfoil," AIAA Paper 2005-5185, 2005.
- [19] Wright, W. B. "Further Refinement of the LEWICE SLD Model," AIAA Paper 2006-464, 2006.
- [20] Wright, W. B., Potapczuk, M. G. Levinson, L.H. "Comparison of LEWICE and Glenn ICE in the SLD Regime," AIAA Paper (2008) No. AIAA-2008-0439.
- [21] Trujillo, M. F., Mathews, W. S., Lee, C. F., and Peters, J. E., "Modeling and Experiment of Impingement and Atomization of a Liquid Spray on a Wall," International Journal of Engine Research, Vol. 1, No. 1, 2000, pp. 87–105.
doi:10.1243/1468087001545281
- [22] Wright, W. B., and Potapczuk, M. G., "Semi-Empirical Modeling of SLD Physics," AIAA Paper 2004-0412, 2004; also NASA TM-2004-212916.
- [23] Papadakis, M., Wong, S. C., Rachman, A., Hung, K. E., Vu, G. T., and Bidwell, C. S., "Large and Small Droplet Impingement Data on Airfoils and Two Simulated Ice Shapes," NASATM2007-213959, Oct. 2007.
- [24] Clift, R., Grace, J. R., Weber, M. E., "Bubbles, Drops and Particles," Academic Press, New York, 1978.
- [25] Roland Schmehl, "Advanced Modeling of Droplet Deformation and Breakup For CFD Analysis of Mixture Preparation," 18th Annual Conference on Liquid Atomization and Spray Systems. ILASS-Europe 2002.

- [26] Gent R. W., Dart N. P. and Cansdale J. T., "Aircraft Icing," *Phil. Trans. R. Soc. Lond. A* 2000 358.
doi: 10.1098/rsta.2000.0689
- [27] Bai, C., and Gosman, A. D., "Development of Methodology for Spray Impingement Simulation," Society of Automotive Engineers Paper 950283, 1995.
- [28] Mundo, C., Tropea, C., and Sommerfeld, M., "Numerical and Experimental Investigation of Spray Characteristics in the Vicinity of a Rigid Wall," *Experimental Thermal and Fluid Science*, Vol. 15, No. 3, 1997, pp. 228–237.
doi:10.1016/S0894-1777(97)00015-0
- [29] Han, Z., Xu, Z., Trigui, N., "Spray/wall Interaction Models for Multidimensional Engine Simulation," *International Journal of Engine Research* 1, 2000, pp.127-146.
doi: 10.1243/1468087001545308
- [30] Papadakis, M., Rachman, A., Wong, S. C., Yeong, H.W., Hung, K. E., Vu, G. T., and Bidwell, C. S., "Water Droplet Impingement on Simulated Glaze, Mixed, and Rime Ice Accretions," NASA TM2007-213961, Oct. 2007.
- [31] Batchelor, G. K., "An Introduction to Fluid Dynamics," Cambridge Univ. Press, Cambridge, England, 1967.
- [32] FLUENT (6.3) User's Guide, Fluent Inc, September 2006.